Progress In Electromagnetics Research M, Vol. 101, 117–126, 2021

Uncertainty Quantification and Parameter Estimation in the Finite-Difference Frequency-Domain Method Using Polynomial Chaos

Andrew C. M. Austin*

Abstract—A new numerical method is proposed for uncertainty quantification in the two-dimensional finite-difference frequency-domain (FDFD) method. The method is based on an intrusive polynomial chaos expansion (PCE) of the Helmholtz equation in terms of the material properties. The resulting PCE-FDFD method is validated against Monte-Carlo simulations for an electromagnetic scattering problem at 1.0 GHz. Good agreement is found between the statistics of the electric fields computed using the proposed method and the Monte-Carlo results, with a factor 15–120 reduction in the computational costs. The PCE-FDFD method is also applied to estimate the material properties from exterior measurements by formulating an objective function and applying constrained optimisation techniques. A maximum 1.7% error in the material properties was observed for a test geometry with six unknowns and 20 sample points.

1. INTRODUCTION

The finite-difference frequency-domain (FDFD) method is a relatively simple, yet highly accurate, frequency-domain technique to numerically solve Maxwell's equations on the Yee mesh [1–3]. In particular — combined with the perfectly matched layer (PML) absorbing boundary condition [1], and total-field/scattered-field sources [2] — two-dimensional implementations of the FDFD method have been widely used as the deterministic 'forward' solvers for electromagnetic inverse scattering and imaging applications [4–6], and for modelling propagation through biological tissue [3, 7].

A significant challenge for numerical electromagnetic techniques, such as the FDFD method, is the inclusion of uncertainties and randomness in the input parameters. In particular, random variations in the material properties or geometry will 'propagate' through a numerical method to introduce uncertainty in the solutions [8]. Quantifying this uncertainty is important for sensitivity analysis, inverse problems, and parameter estimation. A *single* simulation run at the nominal values (or otherwise) will not capture this information. Currently, the Monte-Carlo method is used to predict uncertainty in electromagnetic simulations. However, Monte-Carlo typically converges slowly and is impractical for large problems, though advances such as multi-level Monte-Carlo can converge faster and have been applied for electromagnetic problems [9].

Recently, computationally efficient methods based on the polynomial chaos expansion (PCE) have been used to characterise uncertainty in computational electromagnetics, e.g., the finite-difference time-domain method [8, 10–16], and the method of moments [17]. Polynomial chaos methods can be broadly divided into *intrusive* and *non-intrusive* formulations. Non-intrusive techniques, such as stochastic collocation, collate a number of deterministic simulation runs and compute the coefficients in the PCE

Received 31 December 2020, Accepted 20 February 2021, Scheduled 25 February 2021
* Corresponding author: Andrew C. M. Austin (a.austin@auckland.ac.nz).
The author is with the Department of Electrical, Computer, and Software Engineering, The University of Auckland, Auckland, New Zealand.

via multi-dimensional quadrature (which can be expensive, unless sparse grid quadrature rules are used) [18–20]. In contrast, *intrusive* PCE expands the governing equations of a numerical method in terms of the basis functions and recasts these using a Galerkin procedure [8, 10, 21]. While the computational costs are increased relative to the non-stochastic case, the intrusive polynomial chaos method converges faster than Monte-Carlo and can provide accurate estimates for the statistics from a *single* simulation run [21, pp. 78–88].

Contributions: This paper proposes a new numerical method based on the application of intrusive PCE to the two-dimensional FDFD method. We derive the new coupled governing equations for the PCE-FDFD method and show how these can be arranged in a matrix to solve for the random electric fields. In particular, we focus on uncertainties arising from random material dielectric properties, i.e., permittivity, ϵ_r, and conductivity, σ, and validate the PCE-FDFD solutions against Monte-Carlo simulations. Of particular relevance to this paper, a similar approach was proposed for the two-dimensional FDFD method in [3] and [7], using Taylor's series expansions for the uncertain parameters. However, the proposed PCE-FDFD method uses polynomial chaos basis functions which capture cross-correlation terms between the uncertain parameters, allowing more accurate statistics and larger variabilities to be considered [11]. Accordingly, another contribution of this paper is to validate the performance of the PCE-FDFD method for parameter estimation, where exterior 'measurements' of the electric fields are used to infer the material properties.

This paper is structured as follows: Section 2 outlines the derivation of the 2D PCE-FDFD method and shows the matrix structure of the coefficients. Section 3 provides a validation of the proposed method against the Monte-Carlo technique. In Section 4 the PCE-FDFD solution is applied to parameter estimation. The paper is briefly concluded in Section 5.

2. DERIVATION OF THE PCE-FDFD METHOD

2.1. Helmholtz Equation

In the frequency domain, the Helmholtz equation for the vector electric field, $\mathbf{E}$, is given by

$$\nabla^2\mathbf{E} = j\omega\mu\sigma\mathbf{E} - \omega^2\mu\epsilon\mathbf{E} \tag{1}$$

where $\omega = 2\pi f$ is the angular frequency, and the waves are assumed to propagate in a medium with permittivity $\epsilon = \epsilon_0\epsilon_r$, permeability $\mu = \mu_0\mu_r$, and conductivity σ. Assuming two-dimensional TM_z polarisation, Eq. (1) can be expressed

$$\frac{\partial^2 E_z}{\partial x^2} + \frac{\partial^2 E_z}{\partial y^2} - \gamma E_z = 0 \tag{2}$$

where $\gamma = j\omega\mu(\sigma + j\omega\epsilon)$. When there is no uncertainty in the material properties Eq. (2) can be solved directly by discretising the problem space and applying finite-difference approximations to the derivatives [1]. The following subsections will discuss how uncertainties in the material properties can be incorporated into Eq. (2) using polynomial chaos.

2.2. The Polynomial Chaos Expansion

Assuming the uncertainties in the permittivity and conductivity for each material can be expressed

$$\epsilon_r\left(\xi_k\right) = \epsilon_r^{nom} + x_{\epsilon_r}\xi_k \tag{3}$$

$$\sigma\left(\xi_{k+1}\right) = \sigma^{nom} + x_{\sigma}\xi_{k+1} \tag{4}$$

where ϵ_r^{nom} and σ^{nom} represent the nominal permittivity and conductivity; ξ_k and ξ_{k+1} are independently distributed random variables; x_{ϵ_r} and x_σ represent the variability. There are a total of K random variables $\boldsymbol{\xi} = \{\xi_1, \xi_2, \ldots, \xi_K\}$, and the polynomial chaos method expands the uncertain E_z fields in Eq. (2) as a truncated summation of multivariate orthogonal basis functions Ψ_a in $\boldsymbol{\xi}$, for example,

$$E_z(\boldsymbol{\xi}) = \sum_{a=0}^{P} e_z^a \Psi_a\left(\boldsymbol{\xi}\right) \tag{5}$$

where e_z^a are the weighting coefficients, which are also functions of space. The number of terms, assuming a total-degree basis, is given by

$$P+1=\frac{(K+D)!}{K!D!} \tag{6}$$

where D is the highest order in the polynomial expansion. The multivariate polynomial chaos basis functions are given by

$$\Psi_a\left(\boldsymbol{\xi}\right)=\prod_{k=1}^{K}\phi_{h_k^a}\left(\xi_k\right), \tag{7}$$

where $\phi_{h_k^a}\left(\xi_k\right)$ is a univariate orthogonal polynomial function in ξ_k, and h_k^a is the k-th element of a multi-index [21, pp. 64–67]. The elements of the multi-index specify the degree of the corresponding univariate polynomials. The multivariate basis functions are orthogonal over the domain Ω with respect to a weight function w, which is the PDF associated with each polynomial family through the Wiener-Askey scheme [21]. The inner products are given by

$$\left\langle\Psi_a\left(\boldsymbol{\xi}\right),\Psi_b\left(\boldsymbol{\xi}\right)\right\rangle=\int_\Omega\Psi_a\left(\boldsymbol{\xi}\right)\Psi_b\left(\boldsymbol{\xi}\right)w\left(\boldsymbol{\xi}\right)d\boldsymbol{\xi}=\left\langle\Psi_a^2\left(\boldsymbol{\xi}\right)\right\rangle\delta_{a,b}. \tag{8}$$

For uniformly distributed random variables, Legendre polynomials are used with $w=0.5^K$ and $\Omega=[-1,1]^K$ [21]. In the presence of uncertainty introduced by randomness in ϵ_r and σ, Eq. (2) can be expressed

$$\frac{\partial^2E_z(\boldsymbol{\xi})}{\partial x^2}+\frac{\partial^2E_z(\boldsymbol{\xi})}{\partial y^2}-\gamma(\boldsymbol{\xi})E_z(\boldsymbol{\xi})=0. \tag{9}$$

Substituting Eq. (5) into Eq. (9) yields

$$\frac{\partial^2\sum_{a=0}^{P}e_z^a\Psi_a\left(\boldsymbol{\xi}\right)}{\partial x^2}+\frac{\partial^2\sum_{a=0}^{P}e_z^a\Psi_a\left(\boldsymbol{\xi}\right)}{\partial y^2}+\gamma(\boldsymbol{\xi})\sum_{a=0}^{P}e_z\Psi_a\left(\boldsymbol{\xi}\right)=0. \tag{10}$$

Applying a Galerkin procedure to Eq. (10) by taking inner products with the test function $\Psi_b(\boldsymbol{\xi})$, where $b=0,\ldots,P$, yields

$$\frac{\partial^2e_z^b}{\partial x^2}\left\langle\Psi_b^2(\boldsymbol{\xi})\right\rangle+\frac{\partial^2e_z^b}{\partial y^2}\left\langle\Psi_b^2(\boldsymbol{\xi})\right\rangle+\sum_{a=0}^{P}e_z^a\left\langle\gamma(\boldsymbol{\xi})\Psi_a(\boldsymbol{\xi})\Psi_b(\boldsymbol{\xi})\right\rangle=0. \tag{11}$$

Discretising Eq. (11) on a regular $N\times M$ grid (with mesh dimensions Δx and Δy), and applying second-order finite-differences leads to

$$\left\langle\Psi_b^2\right\rangle\frac{e_z^b|_{n+1,m}-2e_z^b|_{n,m}+e_z^b|_{n-1,m}}{\Delta x^2}+\left\langle\Psi_b^2\right\rangle\frac{e_z^b|_{n,m+1}-2e_z^b|_{n,m}+e_z^b|_{n,m-1}}{\Delta y^2}\ldots$$
$$+\sum_{a=0}^{P}e_z^a|_{n,m}\left\langle\gamma(\boldsymbol{\xi})|_{n,m}\Psi_a(\boldsymbol{\xi})\Psi_b(\boldsymbol{\xi})\right\rangle=0 \tag{12}$$

for $b=0\ldots P$, where $n=1\ldots N$, and $m=1\ldots M$, are the spatial indices in the x and y direction, respectively.

2.3. Matrix Structure

Equation (12) can be put into matrix form

$$\mathbf{Ax}=\mathbf{b} \tag{13}$$

where $\mathbf{A}\in\mathcal{C}^{NM(P+1)\times NM(P+1)}$ is a matrix of the coefficients in Eq. (12), $\mathbf{x}\in\mathcal{C}^{NM(P+1)}$ a vector of the $e_z|_{n,m}^a$ coefficients, and $\mathbf{b}\in\mathcal{C}^{NM(P+1)}$ the source vector. Plane-wave incidence can be implemented by dividing the mesh into total-field and scattered-field regions and calculating the necessary source

correction-terms for $\mathbf{b}$ [2]. It should be noted that sources are only applied to the $b = 0$ coefficient. The set of equations described by Eq. (12) can be viewed as $P + 1$ FDFD computational meshes for each of the $e_z|_{n,m}^b$ weighting coefficients, where these are interlinked by the $\langle \gamma(\boldsymbol{\xi})|_{n,m} \Psi_a(\boldsymbol{\xi}) \Psi_b(\boldsymbol{\xi}) \rangle$ inner product terms. In spatial regions where there is no uncertainty, the inner product reduces to

$$\gamma|_{n,m} \langle \Psi_a(\boldsymbol{\xi}) \Psi_b(\boldsymbol{\xi}) \rangle = \begin{cases} \gamma|_{n,m} \left\langle \Psi_b^2(\boldsymbol{\xi}) \right\rangle & \text{for } a = b \\ 0 & \text{otherwise.} \end{cases} \tag{14}$$

For regions where there is uncertainty in ϵ_r and σ the inner products in Eq. (12) need to be numerically computed using multivariate quadrature [8]. Fig. 1 shows the structure of the $\mathbf{A}$ matrix. In this example the expansion is truncated after 3 terms. The resulting linear system of equations are solved in Matlab to find the coefficients. To numerically absorb outgoing waves a PML as detailed in [1] is implemented. It should be noted that the PML does not alter the structure of the $\mathbf{A}$ matrix; however, it does need to be implemented for each of the $P + 1$ coefficients. A maximum reflection error of 0.2% was observed for a 12-cell thick PML for each coefficient.

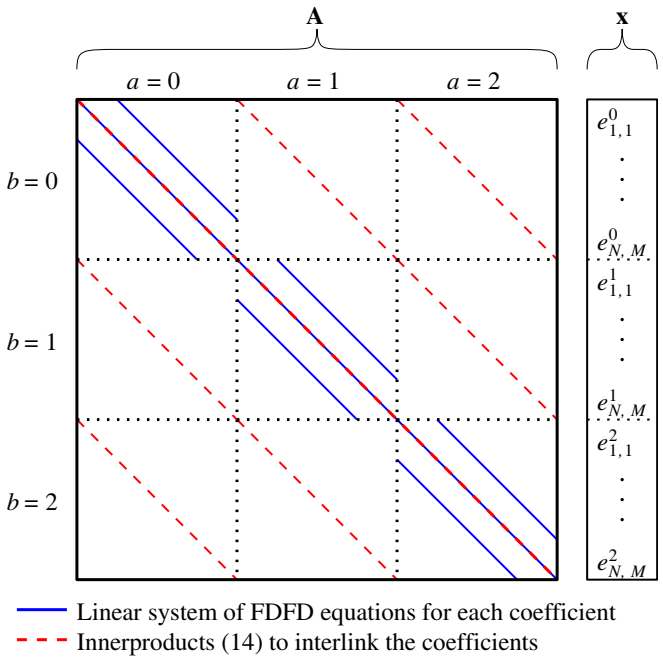

Figure 1. Structure of the $\mathbf{A}$ matrix and $\mathbf{x}$ vector for the proposed PCE-FDFD method. Uncoloured regions in $\mathbf{A}$ represent zeros.

3. VALIDATION EXAMPLE

Figure 2 shows the two-dimensional geometry considered to validate the PCE-FDFD method. The geometry consists of three nested cylinders with different dielectric properties, uncertainty, and radii: $r_1 = 0.3\,\text{m}$ and $r_2 = r_3 = 0.11\,\text{m}$. The uncertainties are assumed to be uniformly distributed and represent a $\pm 20\%$ variation from the nominal values. The source is a 1.0 GHz planewave travelling in the $+x$ direction [2]. The mesh size is $\Delta x = \Delta y = 0.005\,\text{m}$ to ensure a sampling density of at least 15 cells per wavelength in the most optically dense medium.

The uncertainty in E_z is computed using the PCE-FDFD method outlined in the previous section. In this example the expansion is truncated at $D = 1$. Fig. 3 shows a surface plot of the e_z^0 coefficient, which represents the mean solution. As expected the lossy dielectric cylinders attenuate the propagating signal. Figs. 4(a)–(f) show the six PCE coefficients corresponding to the permittivity and conductivity of each cylinder. These surface plots show the contribution each material property makes toward the overall uncertainty in the electric field. For example, Fig. 4(c) shows the uncertainty introduced by the

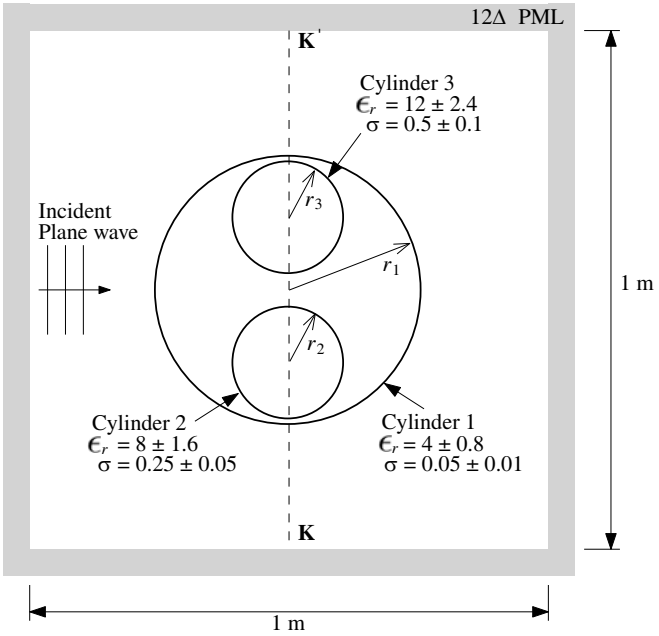

Figure 2. Geometry considered for the TM_z validation example. The uncertainty in ϵ_r and σ for each cylinder is indicated.

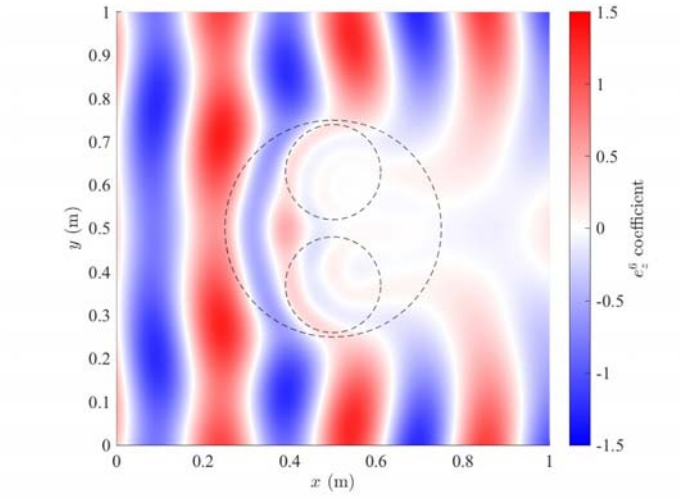

Figure 3. Surface plot of the e_z^0 coefficient from the PCE-FDFD solution. The position of the cylinders is indicated by ---.

permittivity of cylinder 2 is most significant (represented by larger values of the coefficient e_z^3) within the cylinder, but also extends outside the bounds and into the scattered region. It is observed that the value of the e_z^3 coefficient is close to zero within cylinder 3 and in regions shadowed by this cylinder. The relative magnitude of each coefficient gives an indication of the sensitivity. In this example, the e_z^1 coefficients are approximately 5 times larger than the remaining coefficients, indicating the permittivity of cylinder 1 dominates the uncertainty in the electric field. Including higher order coefficients introduces cross-correlation between the parameters, leading to more accurate estimates of the uncertainty in E_z. Sobol indices can also be used for sensitivity analysis to quantify the contribution of each parameter

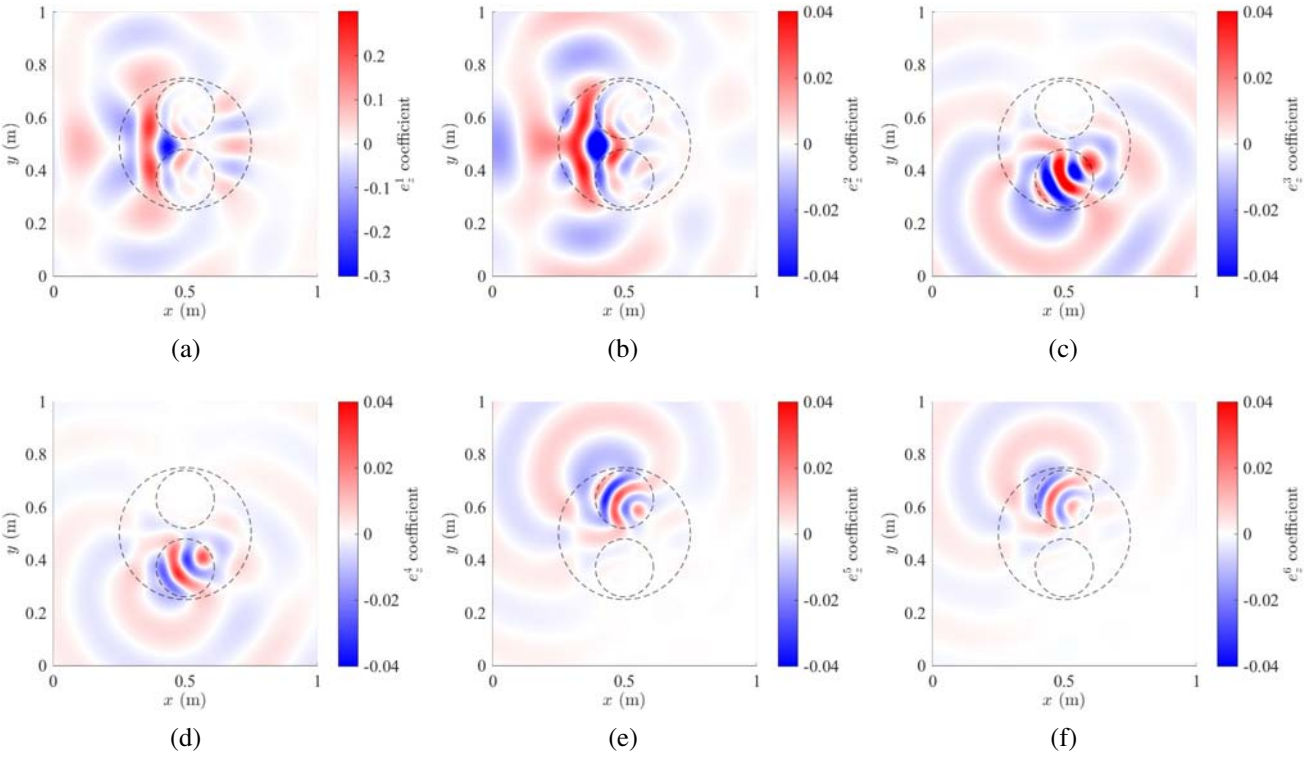

Figure 4. Coefficients of the PCE-FDFD for an expansion truncated at $D = 1$: (a) ϵ_r, cylinder 1; (b) σ, cylinder 1; (c) ϵ_r, cylinder 2; (d) σ, cylinder 2; (e) ϵ_r, cylinder 3; (f) σ, cylinder 3.

toward the overall uncertainty [22]. The Sobol indices for the set of inputs u can be expressed

$$S_u = \frac{\sum_{m \in K_u}^{P} (e_z^m)^2 \left\langle \Psi_m^2 \right\rangle}{\sum_{m=1} (e_z^m)^2 \left\langle \Psi_m^2 \right\rangle}, \tag{15}$$

where K_u is an index to the terms the basis functions that contain u [22].

The PCE-FDFD solution can be used to extract statistics of the electric field [8]. Fig. 5(a) shows the real part of electric field at 1.0 GHz recorded along the line **KK′** in Fig. 2. The field from 20 random realisations of the material properties are overlaid in grey to qualitatively show the variability. The mean electric field is computed using the PCE-FDFD method truncated at $D = 1$ and $D = 2$ and excellent agreement is found for both when compared to 1000 Monte-Carlo trials. Similarly, Fig. 5(b) shows the standard deviation in the electric field along **KK′**, and, consistent with Fig. 5(a), greater variation is observed within the cylinders compared to the region outside. In this case, increasing D improves the accuracy between the standard deviation calculated using the PCE-FDTD method and Monte-Carlo simulations. Fig. 5(c) shows the normalised Sobol indices — indicating the relative contribution each parameter makes toward the uncertainty, computed using Eq. (15) — for each of the six random parameters along the line **KK′** for the $D = 2$ PCE-FDFD results. Similar to the observations from Fig. 4, the dominant source of uncertainty changes along **KK′**. For example: the uncertainty in the $|E_z|$ field outside the cylinders ($0\,\text{m} < y < 0.25\,\text{m}$) is largely dominated by the permittivities of cylinder 1 and 2; within cylinder 2 ($0.25\,\text{m} < y < 0.45\,\text{m}$) the permittivity and conductivity of cylinder 2 dominate; in the central region ($0.45\,\text{m} < y < 0.55\,\text{m}$) the permittivity and conductivity of cylinder 1 are more significant; and similarly for $y > 0.55\,\text{m}$ the material properties of cylinder 3 are observed to contribute toward the uncertainty, while the contributions from cylinder 2 are reduced.

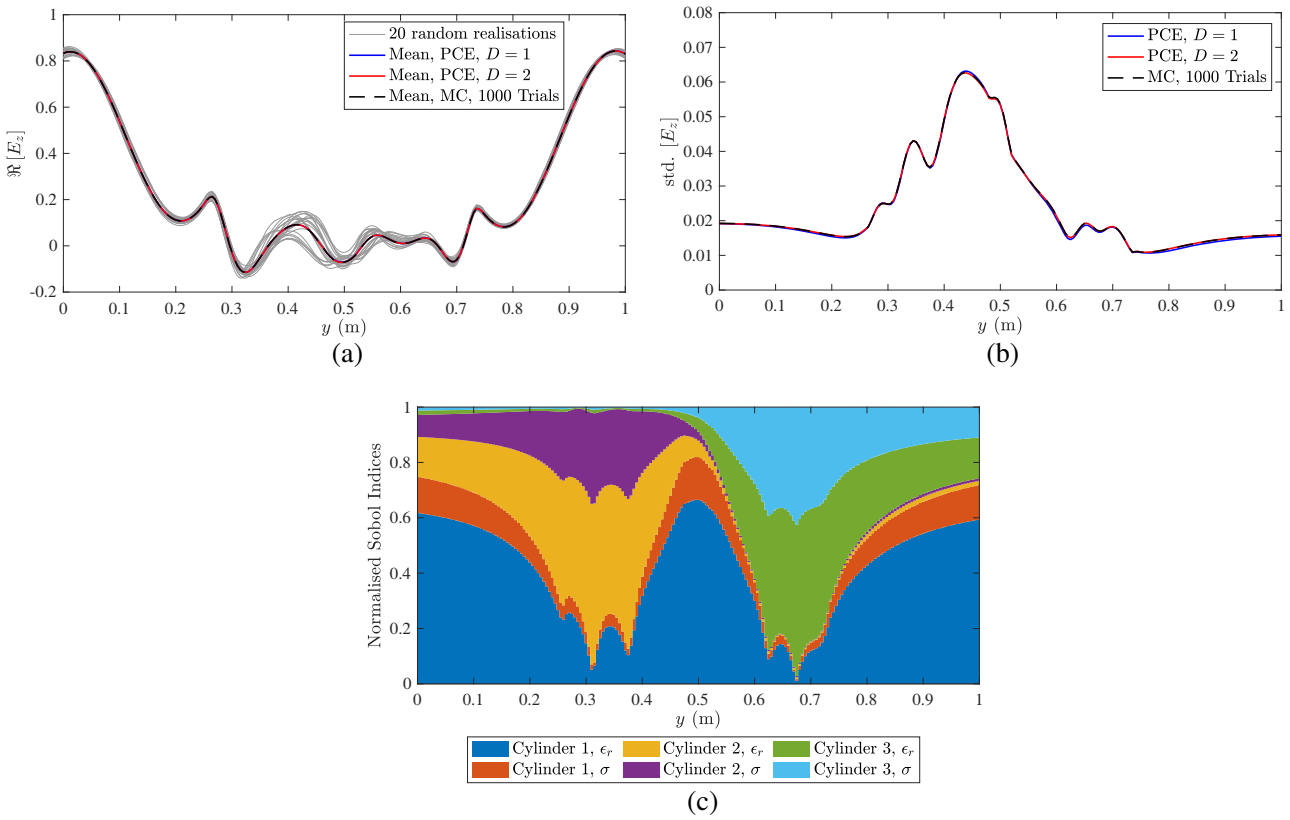

Figure 5. (a) E_z field along $\mathbf{KK'}$ for 20 random realisations, and the mean predicted using the PCE-FDFD for $D = 1$ and $D = 2$ and 1000 Monte-Carlo trials. (b) Standard deviation in the E_z field along $\mathbf{KK'}$ using $D = 1$ and $D = 2$ and 1000 Monte-Carlo trials. (c) Normalised Sobol indices for each parameter along $\mathbf{KK'}$ for $D = 2$.

For the example presented, each Monte-Carlo trial takes approximately 7.3 s (on a 2.5 GHz 32 core Intel Xeon E7-8867 processor); for 1000 trials this is approximately 2 hours. In comparison the PCE-FDFD method takes 60 s and 477 s for $D = 1$ and $D = 2$ respectively, representing a factor 15–120 reduction in the computation time. For this example 1000 Monte-Carlo trials are used to compare the computational costs, as it was found this number produces a similar level of accuracy to the PCE-FDFD method (when both are compared against 10,000 Monte-Carlo trials). It should also be noted that for this example the PCE-FDFD method is faster than a stochastic-collocation approach, which would require 85 simulations for an expansion truncated at $D = 2$ (using Gauss-Legendre quadrature and Smolyak sparse grids) [18].

4. PARAMETER ESTIMATION USING THE PCE-FDFD METHOD

In this paper we consider a limited parameter estimation problem where we do not have knowledge of the material properties in Fig. 2 (the geometry is assumed to be known) and wish to estimate these based on a limited set of samples of the electric field in the space exterior to cylinder 1. The set of samples is given by $E_z^{\text{obs}}|_{j\in J}$ where j is the index and J samples are used. A standard FDFD method is used to compute E_z^{obs} with the 'true' set of material properties.

Using Legendre polynomials in the PCE-FDFD method, we essentially 'solve' a forward problem over the entire input parameter space spanned by the range of uncertainties. That is, the electric field is expressed as a weighted summation of the basis functions in each of the material properties. Accordingly, by comparing the PCE-FDFD solution to $E_z^{\text{obs}}|_{j\in J}$ at the same points we can determine an estimate for the set of material properties. Formally, the objective function, $\mathcal{E}$, representing the

difference between the observed fields E_z^{obs} at J locations in the mesh and the PCE-FDFD solution can be written

$$\mathcal{E}(\boldsymbol{\xi}) = \sum_{j \in J} \left| \sum_{a=0}^{P} e_z^a|_j \Psi_a(\boldsymbol{\xi}) - E_z^{\text{obs}}|_j \right|. \tag{16}$$

It should be noted that Eq. (16) is a function of the K random variables, $\boldsymbol{\xi} = \{\xi_1, \xi_2, \ldots, \xi_K\}$, over the domain $[-1, +1]^K$. Accordingly constrained minimisation (using the Matlab implementation of the interior-point algorithm) can be used to find the values of $\boldsymbol{\xi}$ that minimise Eq. (16) and thus estimate the material properties using Eqs. (3) and (4).

Figure 6 plots the percentage error between the six 'true' and estimated material properties considered in Fig. 2, as the number of sample points is increased. The PCE-FDFD method truncated at $D = 2$ and the error is averaged over 1000 random realisations. The sample points are evenly spaced on a circle 0.15 m from the surface of cylinder 1 (in the total field region). It is observed that the error generally decreases as J increases from 5 to 20 sample points, with no significant improvement beyond 20 samples. For all material properties the error in the estimate is below 1.7% for ≥ 20 sample points. It should be noted that only one run of the PCE-FDFD method is required to generate the $a = 0, \ldots, P$ e_z^a coefficients in Eq. (16).

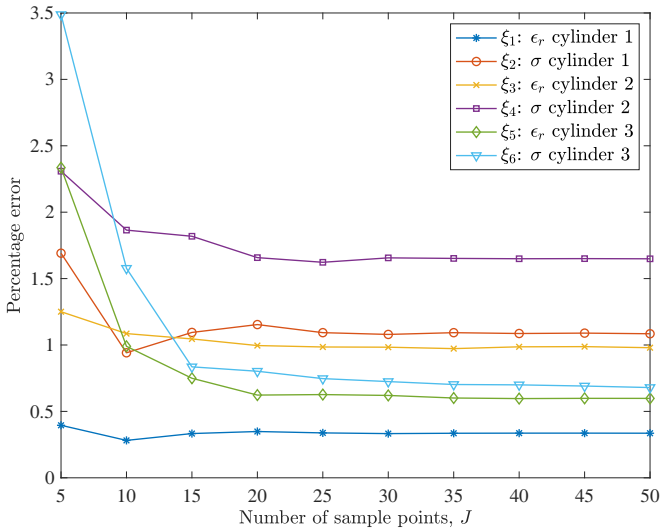

Figure 6. Error in the material parameters estimated using the PCE-FDFD method ($D = 2$) compared to the 'true' solutions (averaged over 1000 trials) as the number of sample points is increased.

5. CONCLUSIONS

The polynomial chaos expansion is applied to the two-dimensional Helmholtz equation and discretised using the FDFD method. A Galerkin procedure is used to recast the coupled equations into a matrix form that can be solved using conventional techniques. The resulting PCE-FDFD method solves for the uncertainty in the time-harmonic electric fields, which are expressed as an expansion of orthogonal polynomial basis functions in the material properties. The statistics of the electric field at 1.0 GHz for a scattering problem with uncertain dielectric properties are computed using the Monte-Carlo method and compared with the PCE-FDFD solution. Good agreement is found when the expansion is truncated at first-order terms; further improvement is observed by increasing the order of the expansion. The reduction in the computational cost is approximately a factor 15–120. Estimates of the material properties from exterior measurements were found by formulating an objective function and applying constrained optimisation techniques. A maximum 1.7% error in the material properties was observed for a test geometry with six unknowns and greater than 20 sample points.

REFERENCES

1. Rappaport, C. M., M. Kilmer, and E. Miller, "Accuracy considerations in using the PML ABC with FDFD Helmholtz equation computation," *International Journal of Numerical Modelling: Electronic Networks, Devices and Fields*, Vol. 13, No. 5, 471–482, 2000.
2. Rumpf, R. C., "Simple implementation of arbitrarily shaped total-field/scattered-field regions in finite-difference frequency-domain," *Progress In Electromagnetics Research B*, Vol. 36, 221–248, 2012.
3. Masumnia-Bisheh, K., K. Forooraghi, and M. Ghaffari-Miab, "Electromagnetic uncertainty analysis using stochastic FDFD method," *IEEE Transactions on Antennas and Propagation*, Vol. 67, No. 5, 3268–3277, 2019.
4. Dong, Q. and C. M. Rappaport, "Microwave subsurface imaging using direct finite-difference frequency-domain-based inversion," *IEEE Transactions on Geoscience and Remote Sensing*, Vol. 47, No. 11, 3664–3670, 2009.
5. Sun, S., B. J. Kooij, and A. G. Yarovoy, "A linear model for microwave imaging of highly conductive scatterers," *IEEE Transactions on Microwave Theory and Techniques*, Vol. 66, No. 3, 1149–1164, 2017.
6. Layek, M. K. and P. Sengupta, "Forward modeling of GPR data by unstaggered finite difference frequency domain (FDFD) method: An approach towards an appropriate numerical scheme," *Journal of Environmental and Engineering Geophysics*, Vol. 24, No. 3, 487–496, 2019.
7. Masumnia-Bisheh, K. and C. Furse, "Bioelectromagnetic uncertainty analysis using geometrically stochastic FDFD method," *IEEE Transactions on Antennas and Propagation*, 2020, doi: 10.1109/TAP.2020.3025238.
8. Austin, A. C. M. and C. D. Sarris, "Efficient analysis of geometrical uncertainty in the FDTD method using polynomial chaos with application to microwave circuits," *IEEE Transactions on Microwave Theory and Techniques*, Vol. 61, No. 12, 4293–4301, 2013.
9. Litvinenko, A., A. C. Yucel, H. Bagci, J. Oppelstrup, E. Michielssen, and R. Tempone, "Computation of electromagnetic fields scattered from objects with uncertain shapes using multilevel Monte Carlo method," *IEEE Journal on Multiscale and Multiphysics Computational Techniques*, Vol. 4, 37–50, 2019.
10. Edwards, R. S., A. C. Marvin, and S. J. Porter, "Uncertainty analyses in the finite-difference time-domain method," *IEEE Transactions on Electromagnetic Compatibility*, Vol. 52, No. 1, 155–163, Feb. 2010.
11. Nguyen, B. T., A. Samimi, S. E. W. Vergara, C. D. Sarris, and J. J. Simpson, "Analysis of electromagnetic wave propagation in variable magnetized plasma via polynomial chaos expansion," *IEEE Transactions on Antennas and Propagation*, Vol. 67, No. 1, 438–449, 2018.
12. Nguyen, B. T., S. E. W. Vergara, C. D. Sarris, and J. J. Simpson, "Ionospheric variability effects on impulsive ELF antipodal propagation about the earth sphere," *IEEE Transactions on Antennas and Propagation*, Vol. 11, No. 66, 6244–6254, 2018.
13. Gorniak, P., "An effective FDTD algorithm for simulations of stochastic EM fields in 5G frequency band," *2018 IEEE 29th Annual International Symposium on Personal, Indoor and Mobile Radio Communications (PIMRC)*, 1417–1421, Bologna, 2018.
14. Zygiridis, T., A. Papadopoulos, N. Kantartzis, C. Antonopoulos, E. N. Glytsis, and T. D. Tsiboukis, "Intrusive polynomial-chaos approach for stochastic problems with axial symmetry," *IET Microwaves, Antennas and Propagation*, Vol. 13, No. 6, 782–788, 2019.
15. Cheng, X., W. Shao, K. Wang, and B.-Z. Wang, "Uncertainty analysis in dispersive and lossy media for ground-penetrating radar modeling," *IEEE Antennas and Wireless Propagation Letters*, Vol. 18, No. 9, 1931–1935, 2019.
16. Liu, J., H. Li, and X. Xi, "General polynomial chaos-based expansion finite-difference time-domain method for analysing electromagnetic wave propagation in random dispersive media," *IET Microwaves, Antennas and Propagation*, Vol. 15, No. 2, 221–228, 2021.

17. Wang, K. C., Z. He, D. Z. Ding, and R. S. Chen, "Uncertainty scattering analysis of 3-D objects with varying shape based on method of moments," *IEEE Transactions on Antennas and Propagation*, Vol. 67, No. 4, 2835–2840, 2019.
18. Xiu, D., "Efficient collocational approach for parametric uncertainty analysis," *Communications in Computational Physics*, Vol. 2, No. 2, 293–309, 2007.
19. Giraldi, L., A. Litvinenko, D. Liu, H. G. Matthies, and A. Nouy, "To be or not to be intrusive? The solution of parametric and stochastic equations — The plain vanilla Galerkin case," *SIAM Journal on Scientific Computing*, Vol. 36, No. 6, A2720–A2744, 2014.
20. Austin, A. C. M., "Wireless channel characterization in burning buildings over 100–1000 MHz," *IEEE Transactions on Antennas and Propagation*, Vol. 64, No. 7, 3265–3269, 2016.
21. Xiu, D., *Numerical Methods for Stochastic Computations: A Spectral Method Approach*, Princeton University Press, Princeton, NJ, 2010.
22. Crestaux, T., O. Le Maıtre, and J.-M. Martinez, "Polynomial chaos expansion for sensitivity analysis," *Reliability Engineering & System Safety*, Vol. 94, No. 7, 1161–1172, 2009.